Science Advances
AAAS

Supplementary Materials for

Chemically induced protein cage assembly with programmable opening and cargo release

Izabela Stupka, Yusuke Azuma, Artur P. Biela, Motonori Imamura, Simon Scheuring, Elżbieta Pyza, Olga Woźnicka, Daniel P. Maskell, Jonathan G. Heddle*

*Corresponding author. Email: jonathan.heddle@uj.edu.pl

Published 5 January 2022, *Sci. Adv.* **8**, eabj9424 (2022)
DOI: 10.1126/sciadv.abj9424

The PDF file includes:

Other Supplementary Material for this manuscript includes the following:

Materials and Methods

Materials

Dithiobismaleimidoethane (DTME), bismaleimidohexane (BMH), Phusion High-Fidelity DNA Polymerase, T4 DNA ligase, GeneJET Plasmid Miniprep Kit, GeneJET Gel Extraction Kit, and HisPur Ni-NTA resin were purchased from Thermo Fisher Scientific. The molecular cross-linkers were reconstituted in dimethyl sulfoxide (DMSO) to 20 mM stock concentration prior to use. Chloro[diphenyl(3-sulfonatophenyl) phosphine] gold(I) sodium salt hydrate was purchased from STREM Chemicals UK and reconstituted in 50 mM Tris-HCl, pH 7.9, 0.15 M NaCl to 10 mM stock concentration before use. Restriction enzymes used for molecular cloning were purchased from New England BioLabs. Isopropyl-beta-D-thiogalactopyranoside (IPTG), dithiothreitol (DTT) and L-cysteine were purchased from VWR. cOmplete ULTRA Tablets Protease Inhibitor Cocktail was from Roche. Ampicillin sodium salt, urea, 20% sodium dodecyl sulfate (SDS) solution, and guanidine hydrochloride (Gdn-HCl) were purchased from Lab Empire. Chloramphenicol was purchased from PanReac AppliChem. Lysosyme, deoxyribonuclease I from bovine pancreas (DNase I), tetracycline, 5,5'-dithiobis-(2-nitrobenzoic acid) (DTNB), glutathione (GSH) and serum from rat were purchased from Sigma Aldrich. pACTet_H-mCherry and pACTet_H-mOrange plasmids containing N-terminally His_6-tagged mCherry or mOrange2 genes under the control of the tetracycline promoter (tet), were kind gifts from Prof. Donald Hilvert (ETH Zurich) and pET21b_TRAP-K35C was synthesized by BioCat GmbH. All the oligonucleotides were synthesized by Sigma Aldrich.

Methods

Molecular cloning

For all cloning steps *E. coli* NEB 5 alpha strain was used. Plasmid sequences were confirmed by Sanger sequencing performed by Eurofins. Tetracycline-inducible protein expression vectors were constructed by subcloning gene segment encoding TRAP(K35C) into pACTet_H-mCherry or pACTet_H-mOrange. The gene for TRAP(K35C) was amplified by PCR using pET21b_TRAP-K35C as a template and oligonucleotides, FW_XhoI_TRAP and RV_MluI_TRAP (see **table S1**), as primers. The amplified PCR product was directly used as a template for the second PCR which introduced the linker gene segment using FW_BsrGI_tev and RV_MluI_TRAP oligonucleotides as primers. The PCR products were cloned into pACTet_H-mCherry or pACTet_H-mOrange via the *Bsr*GI and *Mlu*I sites to give pACTet_H-mCherry-TRAP-K35C and pACTet_H-mOrange-tev-TRAP-K35C. TRAP used for cage construction contained only a single mutation, K35C, crucial for the subunits linkage as the R64S mutation used in previous TRAP-cage constructs is not required for cage formation (*25*). In detail, earlier work, TRAP used for cage construction contained both K35C And R64S mutations with the latter not required for cage formation (25) but was added for cage forming reactions that were carried out using gold nanoparticles (rather than

TPPMS-Au(I)-Cl). In this work we initially proved cross-linking using the K35C/R64S mutant subsequently moving to the K35C only mutant.

Protein expression and purification

TRAP(K35C/R64S) was produced using *E. coli* strain BL21(DE3) cells that were transformed with pET21b_TRAP-K35C R64S a similar protocol as described previously (*25*) with the addition of 2 mM DTT in buffers during the initial purification steps to avoid undesired cysteine oxidation. The protein was purified by the following method: In brief *E. coli* strain BL21(DE3) cells were transformed with pET21b_TRAP-K35C R64S (see **table S2**). Cells were grown in 1 L LB medium supplemented with ampicillin at 37 °C and shaken until OD_{600} = 0.5-0.7. Protein expression was then induced by addition of 0.5 mM IPTG and cells further shaken for 4 hours. Cells were then harvested by centrifugation for 20 min at 5,000 × g and cell pellets stored at -80 °C until purification. Pellets were resuspended in 50 ml lysis buffer (50 mM Tris-HCl, 50 mM NaCl, pH 7.9) supplemented with DNase I, 1 tablet of protease inhibitor cocktail and 2 mM DTT and stirred for 30 min at room temperature. Then, the samples were sonicated and clarified by centrifugation at 20,000 × g, 4 °C for 25 min. The supernatant fraction was heated at 70 °C for 10 min, and centrifuged again at 20,000 x g for 25 min at 4 °C. The supernatant fraction was purified by ion-exchange chromatography on an ÄKTA purifier (GE Healthcare Life Sciences) using 4 × 5 ml HiTrap QFF column with binding in 50 mM Tris-HCl, pH 7.9, 50 mM NaCl, 2 mM DTT buffer and eluting with a 50 mM–1 M NaCl gradient. Fractions containing TRAP were pooled and concentrated using Amicon Ultra 50 kDa MWCO centrifugal filter units (Millipore). The sample was then subjected to size-exclusion chromatography (SEC) on a HiLoad 26/600 Superdex 200pg column in 50 mM Tris-HCl, pH 7.9, 150 mM NaCl at room temperature. Protein purity was checked by SDS-PAGE and protein concentration was determined by absorbance measured at 280 nm using Nanodrop ND-1000 spectrophotometer (NanoDrop Technologies).

In order to produce patchwork TRAP rings, *E. coli* strain BL21(DE3) cells were co-transformed with either pACTet_H-mOrange-TRAPK35C or pACTet_H-mCherry-TRAP-K35C and pET21_TRAP-K35C (see **table S2**). Cells were grown in 100 ml LB medium supplemented with ampicillin and chloramphenicol at 37 °C until OD600 = 0.5-0.7. At this point, protein expression was induced by addition of 0.2 mM IPTG and 10 ng/ml of tetracycline in the case of pACTet_H-mCherry-TRAP-K35C or 30 ng/ml of tetracycline in the case of pACTet_H-mOrange-TRAP-K35C, followed by incubation for 20 hours at 25 °C. Cells were then harvested by centrifugation for 10 min at 5,000 × g. Cell pellets were stored at -80 °C until purification. Pellets were resuspended in 40 ml lysis buffer (50 mM sodium phosphate buffer, 600 mM NaCl, 10 mM imidazole, pH 8 supplemented with DNase I, lysozyme, 1 tablet of protease inhibitor cocktail, and 2 mM DTT and stirred for 30 min at room temperature. Then, the samples were sonicated and clarified by centrifugation at 10,000 × g, 4 °C for 20 min. The supernatant was then incubated with 4 ml Ni-NTA resin previously equilibrated in lysis buffer in a gravity flow column for 20 min. The resin was then washed more than 10 column volumes of lysis buffer containing 20 and 40 mM imidazole. His-tagged proteins were eluted using 5 ml of 50 mM sodium phosphate buffer containing 500 mM imidazole (pH 8). Protein samples were then buffer exchanged using Amicon Ultra-15 centrifugal filter units (50k molecular weight cut-off (MWCO), Merck Millipore) into 2× phosphate buffered saline (PBS) plus 5 mM ethylenediaminetetraacetic acid (EDTA), referred to as 2×PBS-E herein after. The proteins were then subjected to size-exclusion chromatography using a Superdex 200 Increase 10/300 GL column (GE Healthcare) at 0.8 ml/min flow rate. The main

peak showing absorption at 548 nm or 587 nm was pooled and concentrated using an Amicon Ultra-15 (50k MWCO). Protein purity was checked by SDS-PAGE and protein concentration was determined by absorbance measured using UV-1900 UV-Vis Spectrophotometer (Shimadzu) using extinction coefficients: $\varepsilon_{mCherry\ 587} = 72000\ M^{-1}\ cm^{-1}$, $\varepsilon_{mOrange\ 548} = 58000\ M^{-1}\ cm^{-1}$ (*31*), $\varepsilon_{TRAP\ 280} = 8250\ M^{-1}\ cm^{-1}$ (http://expasy.org/tools/protparam.html). Proteins were stored at 4 °C until use.

Free thiol concentration measurement

Free thiol concentration of either TRAP-cage^{DTME} and TRAP-cage^{BMH} were assessed using 5,5'-dithiobis-(2-nitrobenzoic acid) (DTNB) reagent according to the supplied protocol. Both samples were concentrated to 0.3 mM using Amicon Ultra-4 centrifugal filter unit (100k MWCO). Absorbance at 412 nm was measured using Spectramax 190 UV/VIS plate reader (Molecular Devices). The concentration of free thiols in the samples was calculated from the molar extinction coefficient of 2-nitro-5-thiobenzoic acid (14150 $M^{-1}\ cm^{-1}$) and was not detectable for TRAP-cage^{DTME} and TRAP-cage^{BMH}.

Negative stain transmission electron microscopy (TEM)

Samples for negative stain TEM were prepared in 2×PBS-E pH 7.4 to a final concentration of 0.05 mg/ml. The sample (4 µl) was placed on previously glow discharged carbon coated copper grids (STEM Co.). Excess solution was removed using filter paper followed by incubation with 3% phosphotungstic acid pH = 8 or 2 % uranyl acetate. Samples were visualized using a JEOL JEM-1230 electron microscope with 80 kV operation. All TEM measurements were repeated at least twice independently. Obtained images were analysed using Image J software.

Dynamic Light Scattering

Dynamic Light Scattering (DLS) was carried out at room temperature on a Zetasizer Nano ZSP instrument (Malvern) using 0.4 µM cross-linked TRAP-cage samples (concentration with respect to TRAP monomer) in PBS pH 7.4 in a quartz cuvette. Experiments were repeated 3 times independently for each sample. Results are given as volume distributions and gave uniform results.

Native PAGE

Native PAGE was carried out using 3–12 % native Bis-Tris gels following the manufacturer's recommendations (Life Technologies). Protein (1 µg) was prepared in native PAGE sample buffer (50 mM BisTris, pH 7.2, 10 % w/v glycerol, 0.004 % w/v bromophenol blue). Electrophoresis was run for 1.5 hours at 150 V at room temperature. As protein standard, unstained NativeMark (Life Technologies) was used. Protein bands were visualized by Instant Blue^{TM} protein stain (Expedeon)

or using Typhoon Trio+ Mode Imager (GE Healthcare) with excitation at 532 nm and the emission at 610 nm.

Tricine - SDS PAGE

Gels and buffers for tricine – SDS PAGE were prepared according to the published protocol (*41*). Protein (2 µg) was prepared in SDS PAGE sample buffer (50 mM Tris, pH 7.0, 10 % w/v glycerol, 0.004 % w/v bromophenol blue, 5 % β-mercapthoethanol, 2.5 % SDS), with 4 M urea addition and heated for 20 min at 95 ºC. Potential carbamylation due to the presence of urea was taken into account but it did not lead to the significant resolution decrease. Electrophoresis was run for 1.5 hours at 100 -150 V at room temperature. As protein standard, PageRuler™ Prestained Protein Ladder (Thermo Scientific) was used. Protein bands were visualized by Instant Blue™ protein stain (Expedeon).

Right/Low Angle Light Scattering

Right/Low Angle Light Scattering (RALS/LALS) measurements were carried out using an Omnisec Reveal (Malvern) instrument and Superose 6 Increase 10/300 GL column at a flow rate of 0.5 ml/min on an ÄKTA Purifier FPLC. For molecular mass assessment, 100 µg of either TRAP-cage^{DTME} or TRAP-cage^{BMH} in PBS pH 7.4 were applied to the column and run through RALS/LALS detection system coupled with refractive index (RI) measurement. The average particle molecular mass was calculated using Omnisec Reveal software with a dn/dc value of 0.185 mL/g and protein concentration estimated by observed RI. The system was calibrated using 500 µg of conalbumin (75 kDa) as a reference on the same column.

Fig. S1.

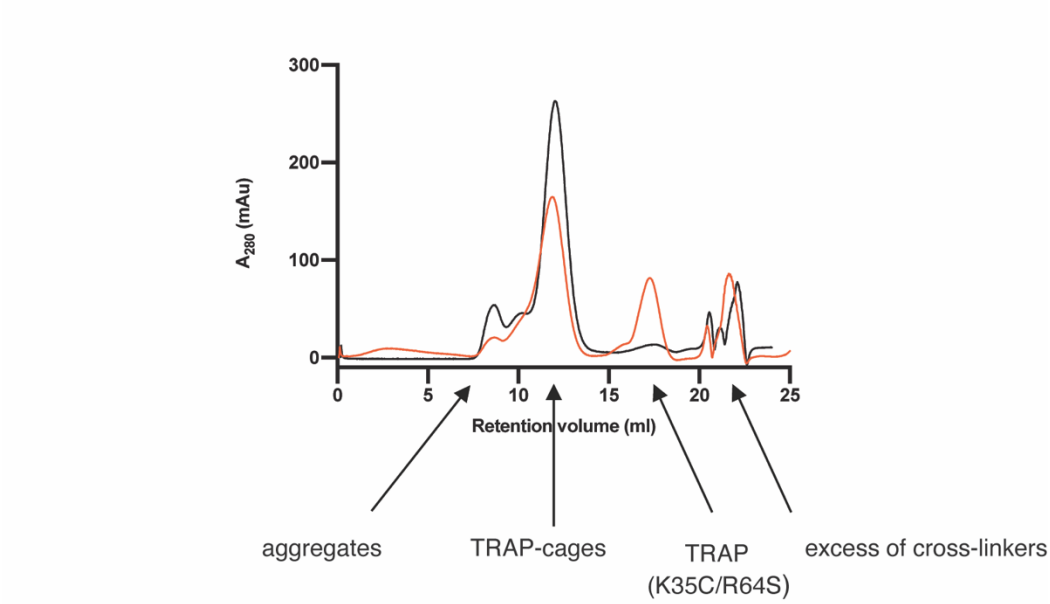

Fig. S1. Results of size-exclusion chromatography after TRAP(K35C/R64S) incubation with DTME (black) or BMH (red) cross-linker after 1 hour incubation. mAU, milli absorbance units.

Fig. S2.

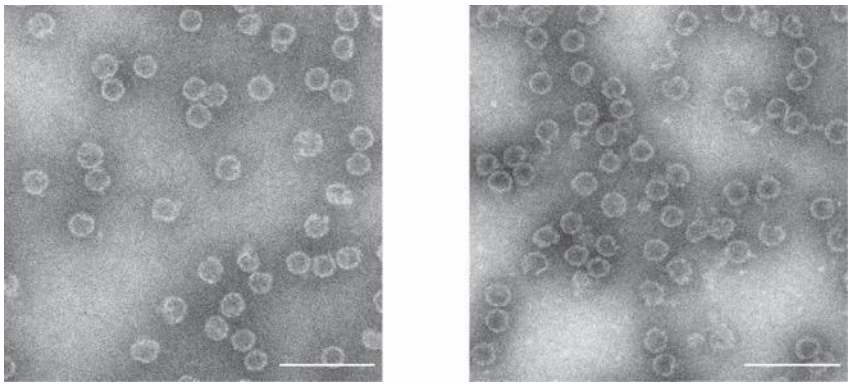

Fig. S2. Transmission electron microscopy (TEM) images of TRAP-cages^{DTME} (right) and TRAP-cages^{BMH} (left). Scale bars, 100 nm.

Fig. S3.

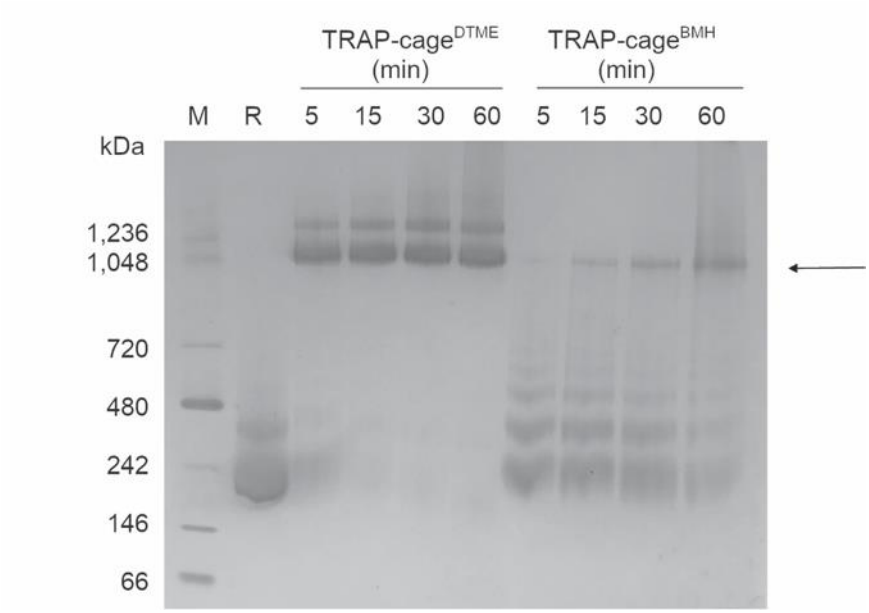

Fig. S3. Kinetics of cross-linked TRAP-cages formation. TRAP(K35C/R64S) run on native PAGE 5-60 min after addition of either DTME or BMH. M, molecular weight marker, R, TRAP(K35C/R64S). Formation of TRAP-cage^{DTME} appears to happen more rapidly than TRAP-cage^{BMH} but results in higher aggregation which can be observed by additional bands seen on the gel and smearing. Black arrow indicates the position of TRAP-cage.

Fig. S4.

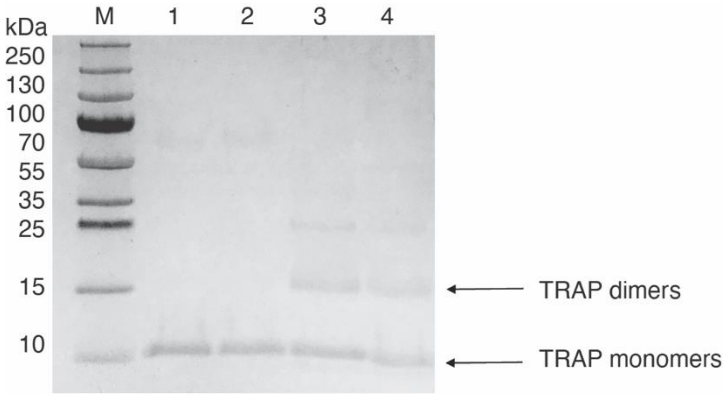

Fig. S4. SDS PAGE of cross-linked TRAP-cages. M, molecular weight marker, lane 1 – TRAP(K35C/R64S), lane 2 - TRAP-cage$^{Au(I)}$, lane 3 - TRAP-cage^{BMH}, lane 4 -TRAP-cage^{DTME} run in non-reducing conditions to visualize cross-linking between the TRAP subunits. SDS PAGE confirms covalent bonds presence in TRAP-cage^{DTME} and TRAP-cage^{BMH}.

Fig. S5.

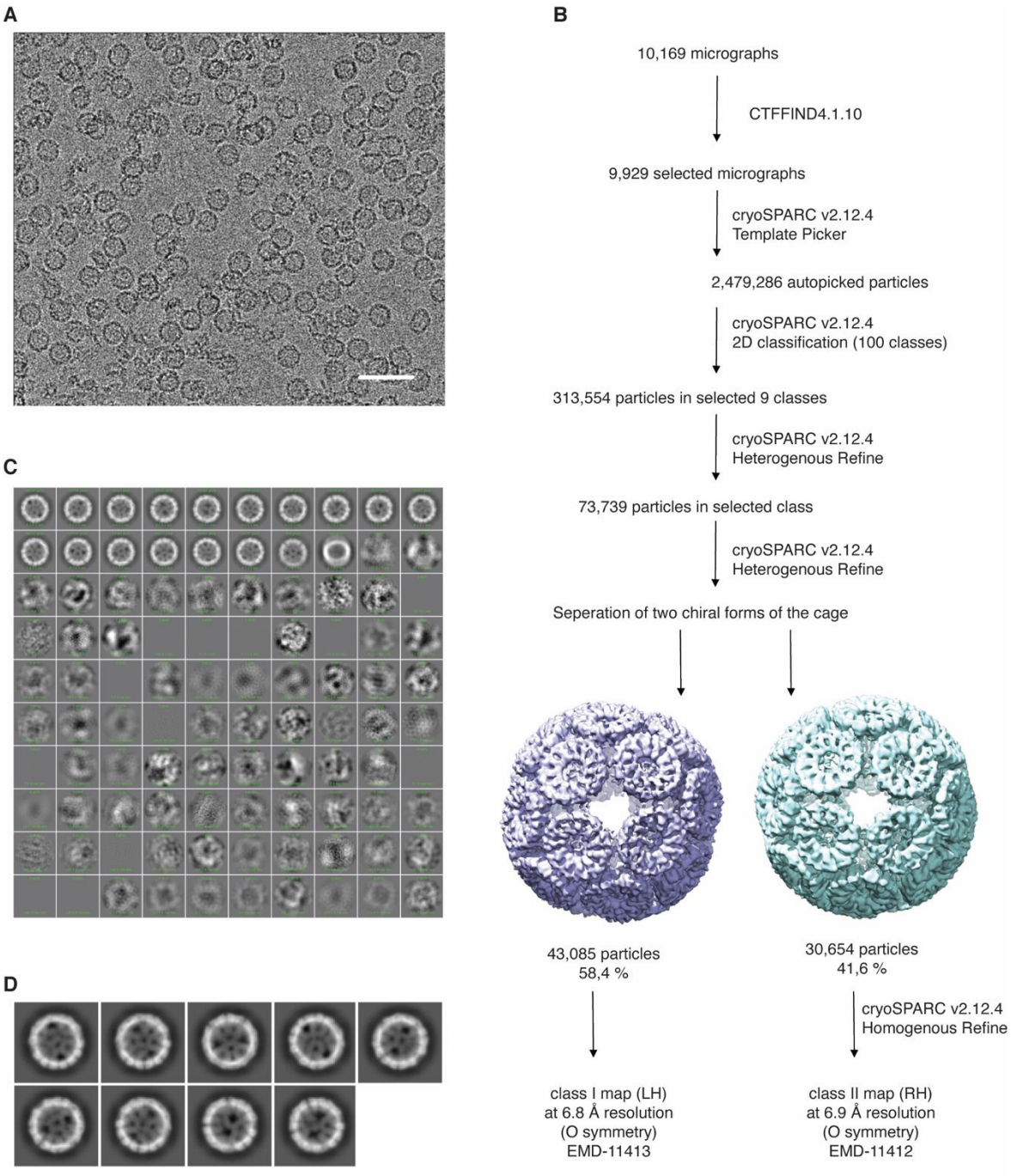

Fig. S5. Procedure for cryo-EM reconstruction of TRAP-cage^{BMH}. (**A**) representative micrograph of the TRAP-cage^{BMH}. Scale bar, 50 nm. **(B**) Summary of the image processing procedure (see Methods). (**C**) 2D class averages from reference-free 2D classification in cryoSPARC v2.12.4. (**D**) Selected nine 2D classes.

Fig. S6.

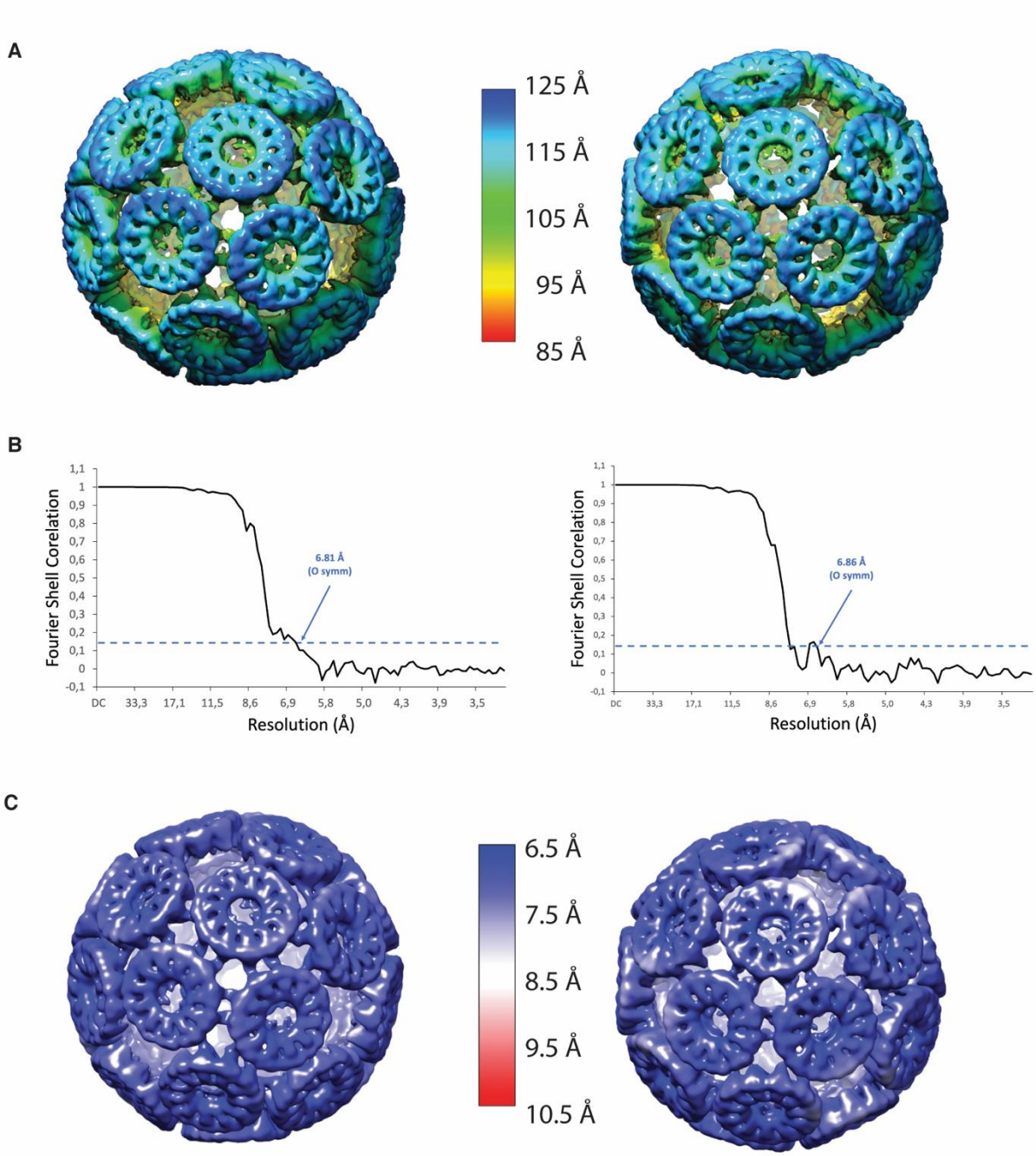

Fig. S6. Map quality and resolution of TRAP-cage^{BMH}. Left and right-handed cages are shown on the left and right, respectively. (**A**) Surface representations coloured according to the distance from the centre of the particle. (**B**) Gold-standard FSC curve for the cryo-EM map of left and right-handed cages with Octahedral (O) symmetry from 43,085 and 30,654 particles, respectively. The estimated resolutions at 0.143 criterion for the maps with octahedral symmetry were 6.81 Å and 6.86 Å respectively. (**C**) The refined density maps coloured by local resolution in surface view.

Fig. S7.

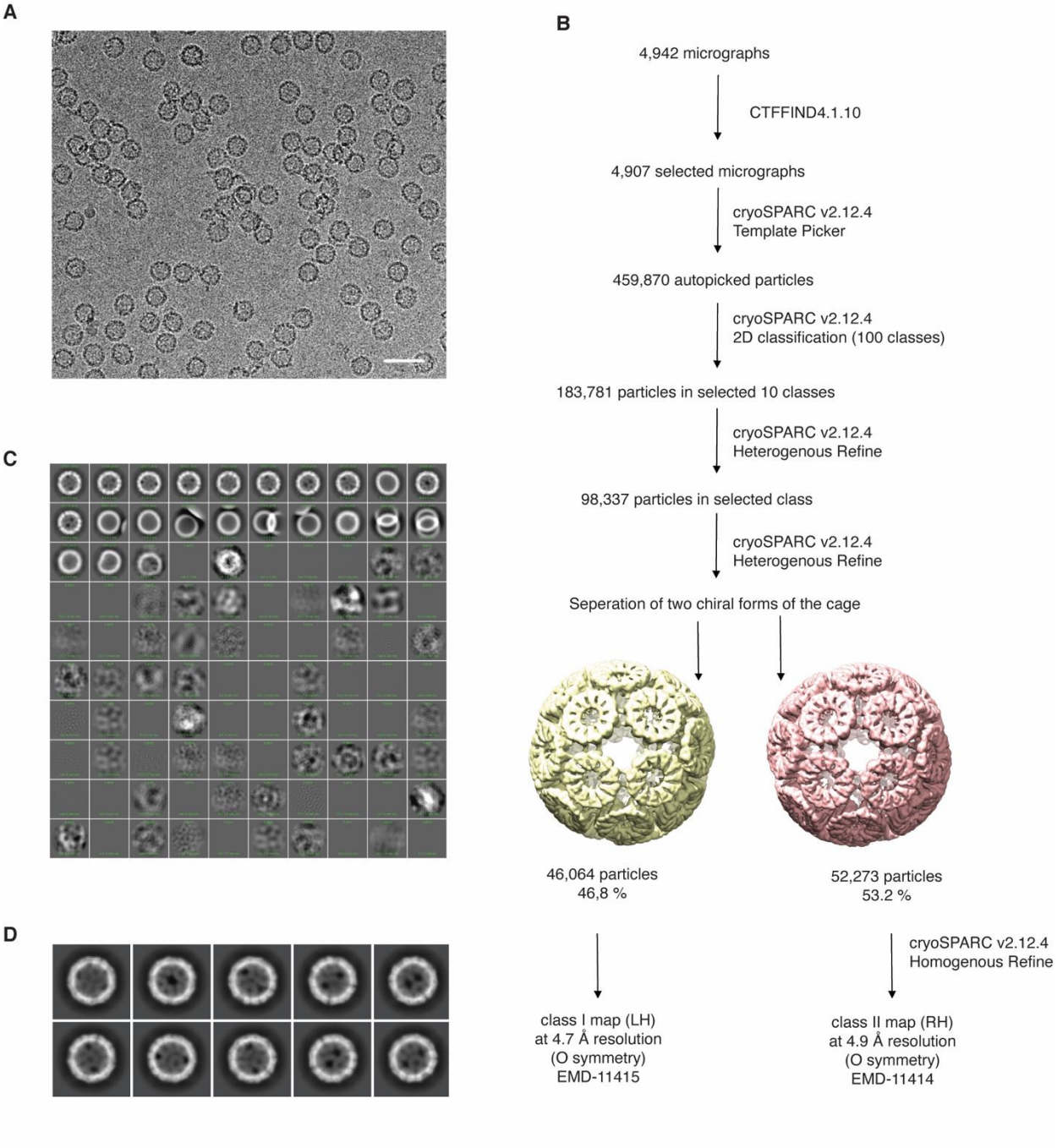

Fig. S7. Procedure for cryo-EM reconstruction of TRAP-cage^{DTME}. (**A**) representative micrograph of the TRAP-cage^{DTME}, Scale bar – 50 nm. (**B**) Summary of the image processing procedure (see Methods). (**C**) 2D class averages from reference-free 2D classification in cryoSPARC v2.12.4. (**D**) Selected ten 2D classes.

Fig. S8.

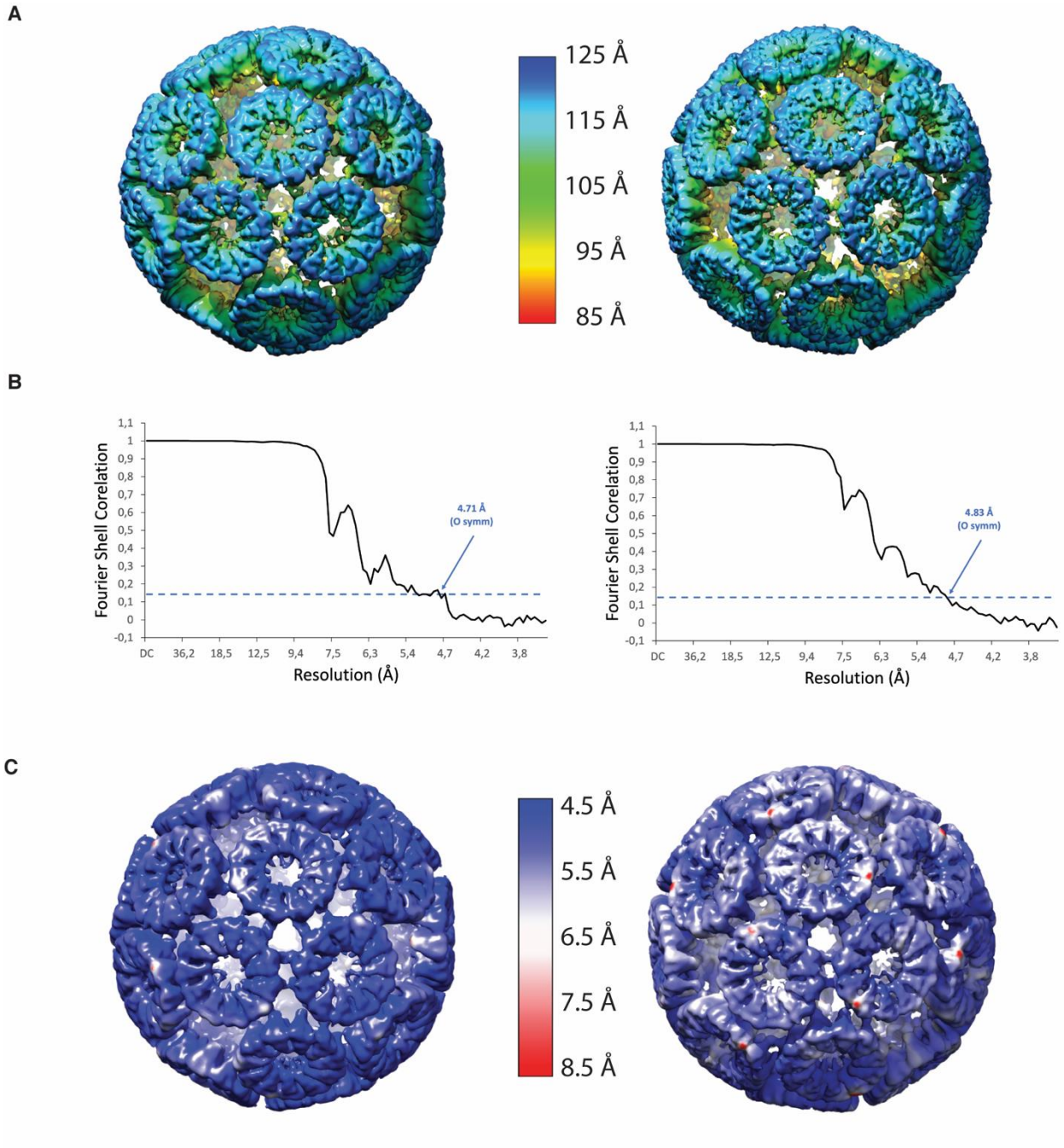

Fig. S8. Map quality and resolution of TRAP-cage^{DTME}. Left and right-handed cages are shown on the left and right, respectively. (**A**) Surface representations coloured according to the distance from the centre of the particle. (**B**) Gold-standard FSC curve for the cryo-EM map of left and right-handed cages with Octahedral (O) symmetry from 46,064 and 52,237 particles, respectively. The estimated resolutions at 0.143 criterion for the maps with octahedral symmetry were 4.71 Å and 4.86 Å respectively. (**C**) The refined density maps coloured by local resolution in surface view.

Fig. S9.

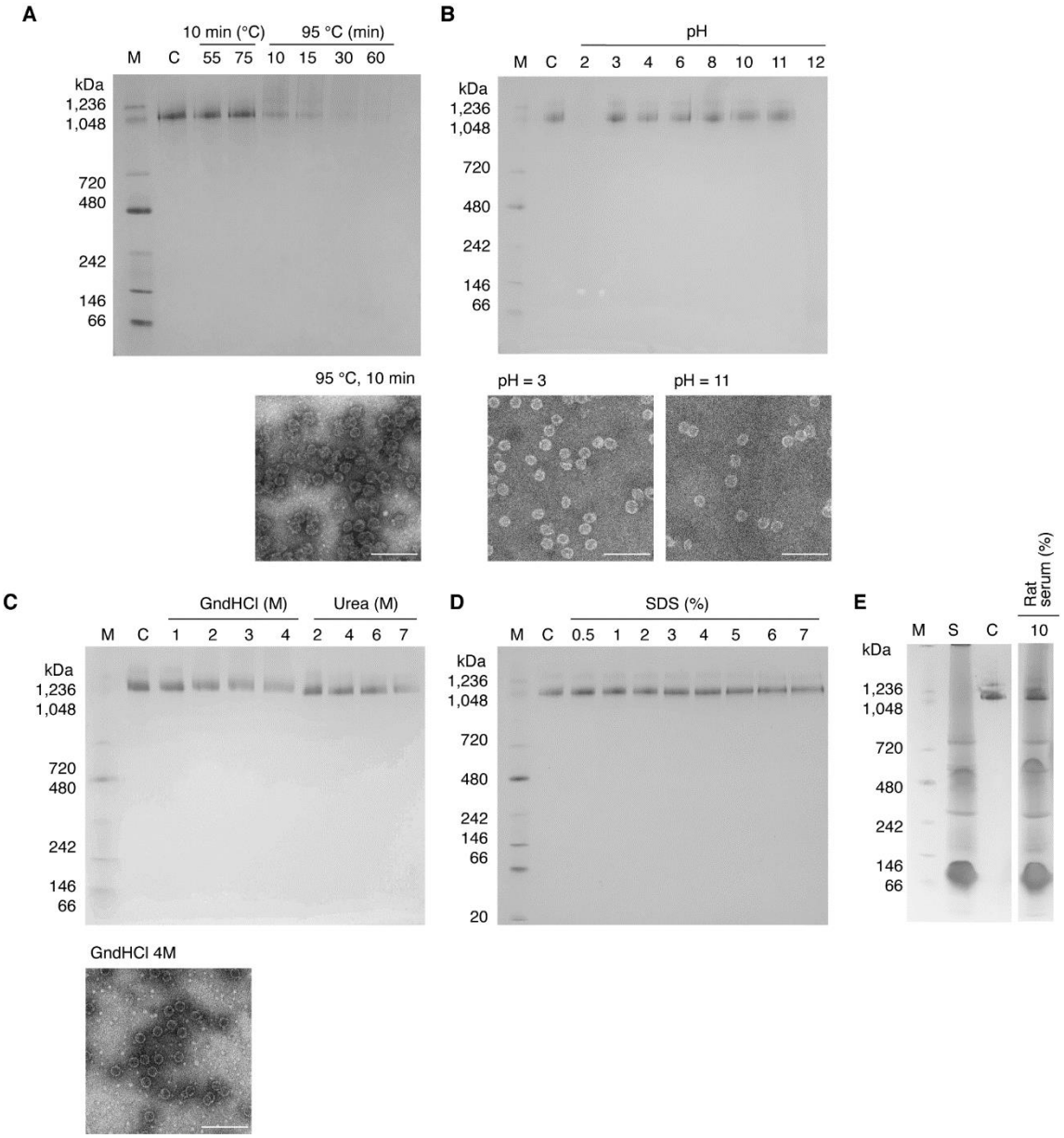

Fig. S9. Stability of TRAP-cage^{DTME}. **(A)** Thermal stability of TRAP-cage^{DTME}. Native PAGE shows preservation of structural integrity at the indicated incubation times and temperatures. TEM image (below) was obtained after incubation at 95 °C for 10 min., scale bar, 100 nm (**B**) Stability as a function of pH. No visible loss of structure was detected from pH 3–11 using native PAGE. TEM images (below) were obtained after incubation at the indicated pH values, scale bar, 100 nm. (**C)** Guanidine hydrochloride (GdnHCl), urea and (**D)** SDS did not affect the structure of TRAP-cage^{DTME} as seen using native PAGE. TEM image (below) was obtained after incubation with 4 M GndHCl, scale bar, 100 nm. (**E**) Native PAGE shows the intactness of the cage after incubation in 10% rat serum. 'C' denotes TRAP-cage^{DTME} and 'S' 10% rat serum control. M = molecular weight marker. Experiments repeated at least 2 times.

Fig. S10.

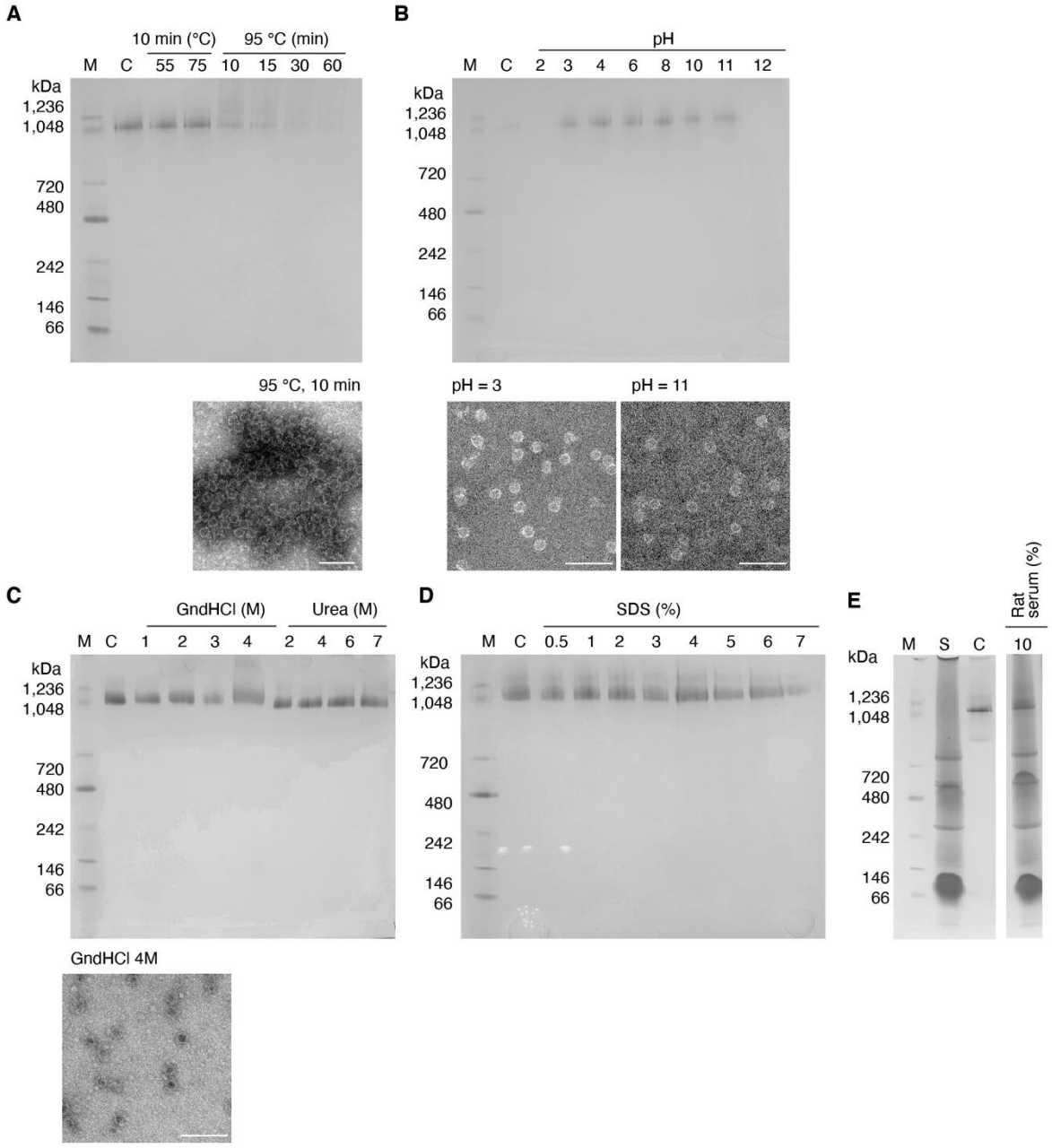

Fig. S10. Stability of TRAP-cage^{BMH}. (**A**) Thermal stability of TRAP-cage^{BMH}. Native PAGE shows preservation of structural integrity at the indicated incubation times and temperatures. TEM image (below) was obtained after incubation at 95 °C for 10 min., scale bar, 100 nm (**B**) Stability as a function of pH. No visible loss of structure was detected from pH 3–11 using native PAGE. TEM images (below) were obtained after incubation at the indicated pH values, scale bar, 100 nm. (**C**) Guanidine hydrochloride (GdnHCl), urea and (**D**) SDS did not affect the structure of TRAP-cage^{BMH} as seen using native PAGE. TEM image (below) was obtained after incubation with 4 M GndHCl, scale bar, 100 nm. (**E**) Native PAGE shows the intactness of the cage after incubation in 10% rat serum. 'C' denotes TRAP-cage^{BMH} and 'S' 10% rat serum control. M = molecular weight marker. Experiments repeated at least 2 times.

Fig. S11.

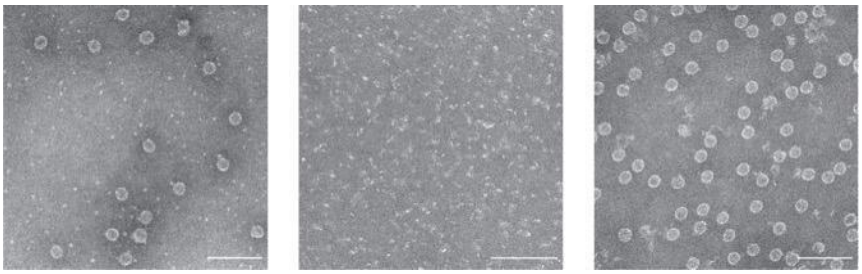

Fig. S11. TEM analysis of the structural intactness and fragmentation of TRAP-cage^{DTME}. Images taken after treatment with 0.1 mM (left) and 1 mM (middle) TCEP, respectively. In contrast, TRAP-cage^{BMH} remains unaffected after treatment with 10 mM TCEP (right). Scale bar, 100 nm.

Fig. S12.

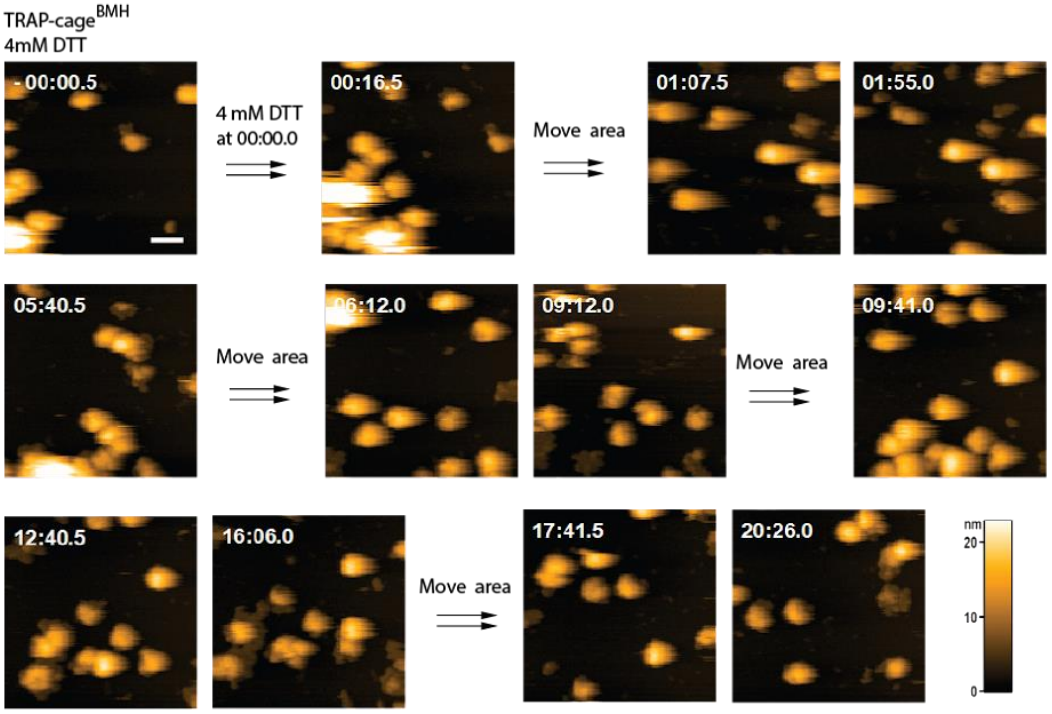

Fig. S12. High-speed atomic force microscopy (HS-AFM) movie showing the effect of 4 mM DTT addition to TRAP-cage^{BMH}. This movie was taken at 2 frames per second, 300 nm x 300 nm, 150 pixel x 150 pixel. Time stamp in the upper left corner of each HS-AFM image indicates the time of frame acquisition after DTT addition. Scale bar at t = -00:00.5 indicates 50 nm. Z colour scale is set to 0 nm to 22 nm (look up table shown bottom right).

Fig. S13.

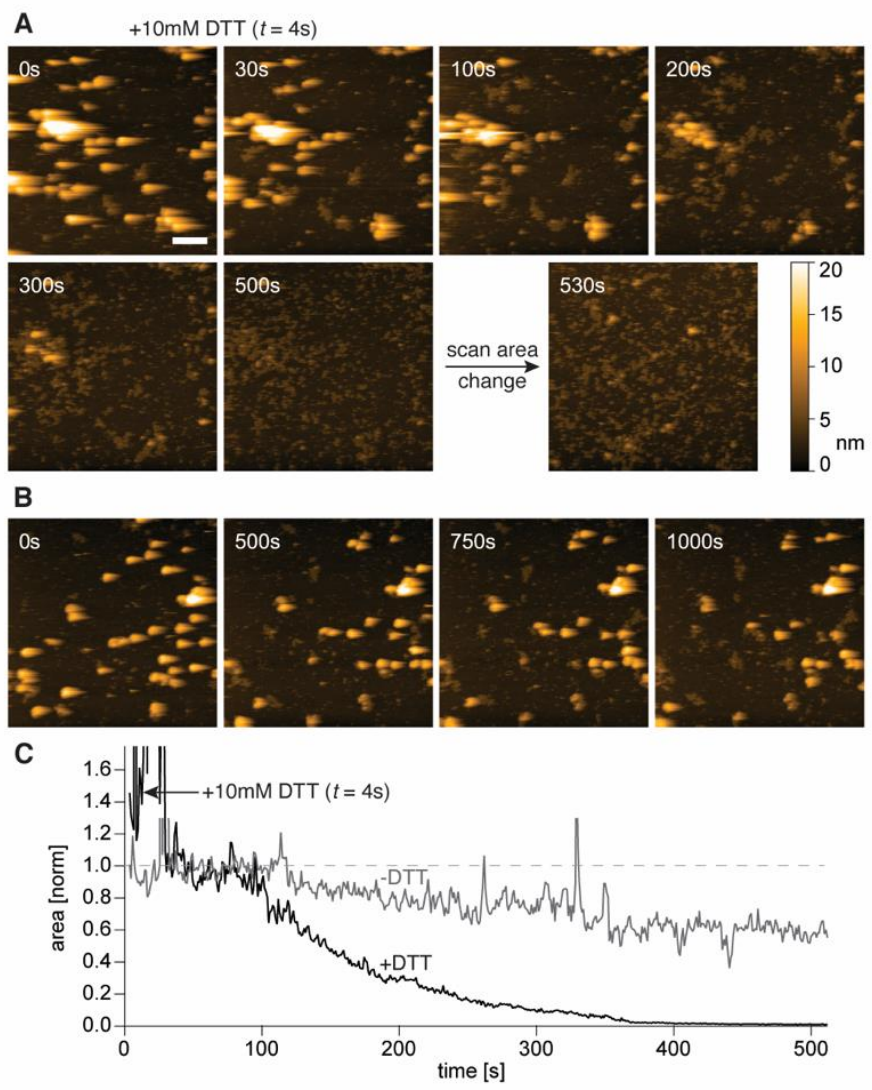

Fig. S13. **High-speed atomic force microscopy (HS-AFM) movies showing the effect of 10 mM DTT addition to TRAP-cage^{DTME} versus control. (A, B)** Selected frames from high-speed atomic force microscopy (HS-AFM) movies of TRAP-cage^{DTME}, taken at 1 frame per second, 600 nm x 600 nm, 200 pixel x 200 pixel, showing the effect of 10 mM DTT addition to TRAP-cage^{DTME} (A), and no effect on cage structure in the absence of DTT (B). Time after DTT addition is indicated. Scale bar at $t = 0$ (in A) indicates 100 nm. Z colour scale is set from 0 nm to 20 nm (look up table shown bottom right in A). (**C**) Plot showing the disappearance of high pixels (>10 nm) indicating the loss of structural integrity as a function of time after addition of 10 mM DTT (black trace), compared to the control experiment in the absence of DTT (gray trace).

Fig. S14.

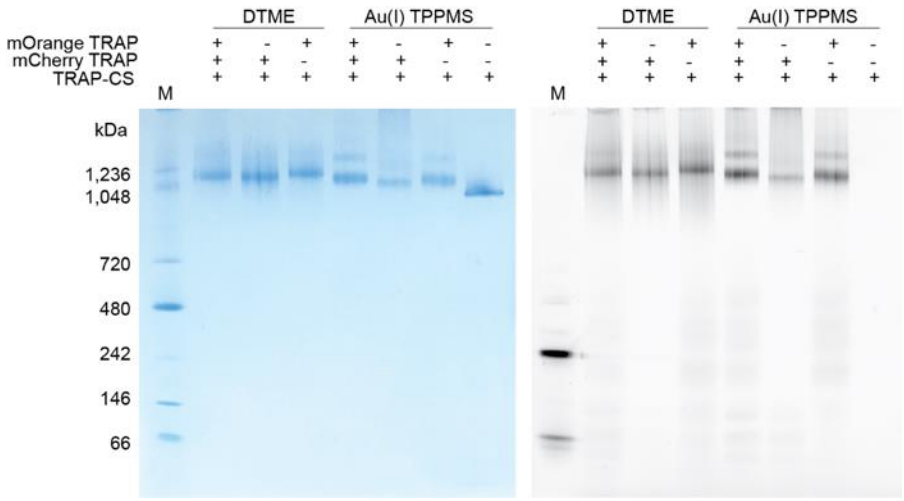

Fig. S14. **Native PAGE showing the fluorescent properties of purified TRAP-cages associated with the fluorescent cargoes**. The gel was visualized using InstantBlue protein staining (right) and fluorescence using excitation at 532 nm and emission at 610 nm (left). M = molecular weight marker.

Fig. S15.

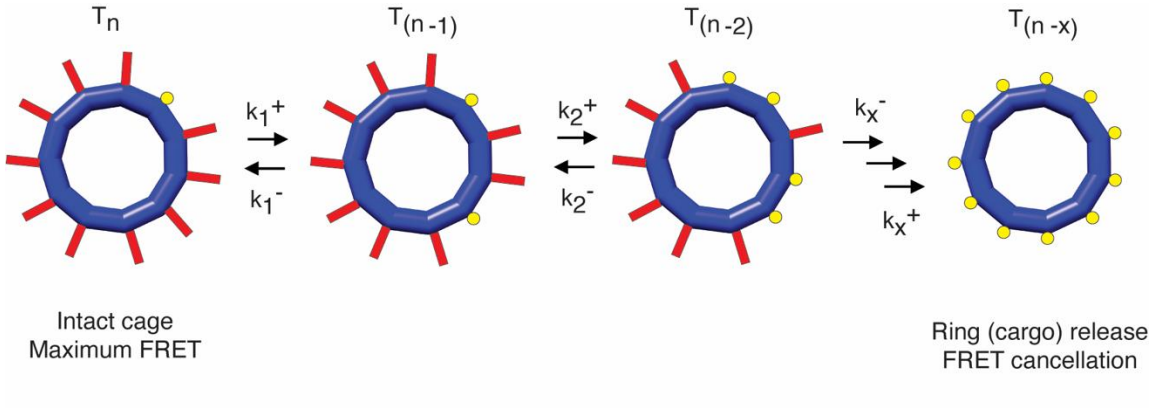

Figure S15. Hypothetical model for TRAP-cage disassembly. The blue ring (T) indicates a TRAP 11-mer in the cage assembly where the cross-linking to form a cage structure (red lines) and the uncross-linked residues (yellow spheres) are highlighted. In both TRAP-cage$^{Au(I)}$ and TRAP-cage^{DTME}, the disassembly caused by DTT can be presented as sequential n×bond cleavage events, where n, and x represent the number of cross-links with neighbors and of bond-cleavage events required for releasing the TRAP 11-mer from the cage assembly, respectively. Assuming critical FRET efficiency change occurs only when the TRAP 11mer is released from the cage assembly, concentration of $T_{(n-x)}$ should corelate to the fluorescence signal change. When the rate of the first few steps in the reaction sequence is similar or faster than that in latter steps, there is a delay in the increase of the concentration of the final product, $T_{(n-x)}$, due to the time required for producing reaction intermediates. When the latter steps in the mechanism become much faster than the first few steps, all the intermediates are rapidly consumed as soon as produced. The overall production rate of $T_{(n-x)}$ depends only on the rate constants in the initial reactions which are the rate determining steps (*42*). The observed pseudo-first-order reaction for the Au(I)-ligand exchange reaction suggests that bond cleavage occurs according to the latter mechanism (Fig. 4C, red circles). The rate-limiting steps are probably the initial ligand exchanges in which opposing pairs of cysteines in the TRAP-cages remain in close proximity, giving a high stability constant with Au(I). In contrast, the delay in the increase of the concentration of $T_{(n-x)}$ for the disulfide shuffling reaction with DTT, which is likely near-irreversible due to its energetically favored six-membered cyclization, indicated that the rate-acceleration is less than that for the metal-ligand exchange (Fig. 4C, black circles).

Fig. S16.

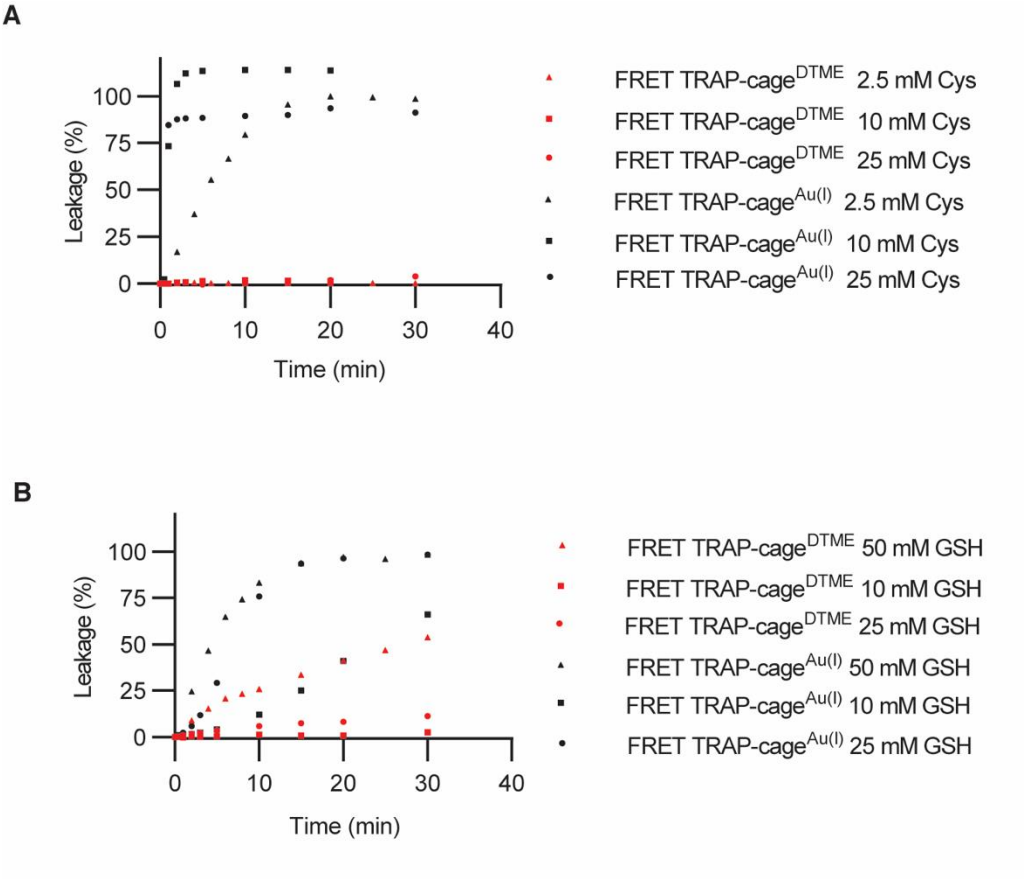

Fig. S16. Time-dependent disassembly of TRAP-cages. (**A, B**) TRAP-cages$^{Au(I)}$ (black) and TRAP-cages^{DTME} (red) after addition of 2.5 mM, 10 mM or 25 mM cysteine (Cys) (A) or 10 mM or 25 mM or 50 mM glutathione (GSH) (B); 100% leakage denotes the highest donor intensity after 10 min of 10 mM DTT treatment.

Table S1. Sequences of oligonucleotides

Name	Sequence
FW_XhoI_TRAP	CTGTACTTCCAGAGCGGCGGTAGCGGCTCGAGCTACACCAACTCTGACTTCGTTG
RV_MluI_TRAP	CTCACGCGTTATTTTTTACCTTCAGATTCGATAACAC
FW_BsrGI_tev	GCTGTACAAGCTTTCTGAAAACCTGTACTTCCAGAGCGGC

Table S2. Plasmids and amino acid sequences

Plasmid name	Plasmid	Gene	Amino acid sequence
pET21b_TRAP-K35C R64S	pET21b	TRAP-K35C R64S	MYTNSDFVVIKALEDGVNVIGLTR GADTRFHHSECLDKGEVLIAQFTE HTSAIKVRGKAYIQTSHGVIESEG KK
pET21b_TRAP-K35C	pET21b	TRAP-K35C	MYTNSDFVVIKALEDGVNVIGLTR GADTRFHHSECLDKGEVLIAQFTE HTSAIKVRGKAYIQTRHGVIESEG KK
pACTet_H-mOrange-TRAP-K35C	pACYC	H-mOrange-TRAP-K35C	MHHHHHHGGSSMVSKGEENNMA IIKEFMRFKVRMEGSVNGHEFEIE GEGEGRPYEGFQTAKLKVTKGGP LPFAWDILSPHFTYGSKAYVKHPA DIPDYFKLSFPEGFKWERVMNYE DGGVVTVTQDSSLQDGEFIYKVKL RGTNFPSDGPVMQKKTMGWEAS SERMYPEDGALKGKIKMRLKLKD GGHYTSEVKTTYKAKKPVQLPGA YIVDIKLDITSHNEDYTIVEQYERA EGRHSTGGMDELYKLSENLYFQS GGSGSSYTNSDFVVIKALEDGVN VIGLTRGADTRFHHSECLDKGEVL IAQFTEHTSAIKVRGKAYIQTRHGV IESEGKK
pACTet_H-mCherry-TRAP-K35C	pACYC	H-mCherry-TRAP-K35C	MHHHHHHGGSSMVSKGEEDNMA IIKEFMRFKVHMEGSVNGHEFEIE GEGEGRPYEGTQTAKLKVTKGGP LPFAWDILSPQFMYGSKAYVKHP ADIPDYLKLSFPEGFKWERVMNF EDGGVVTVTQDSSLQDGEFIYKV KLRGTNFPSDGPVMQKKTMGWE ASSERMYPEDGALKGEIKQRLKLK DGGHYDAEVKTTYKAKKPVQLPG AYNVNIKLDITSHNEDYTIVEQYER AEGRHSTGGMDELYKLSENLYFQ SGGSGSSYTNSDFVVIKALEDGV NVIGLTRGADTRFHHSECLDKGE VLIAQFTEHTSAIKVRGKAYIQTRH GVIESEGKK

Table S3. Average size of cross-linked TRAP-cages determined by dynamic light scattering

	TRAP-cage^{BMH}	
	PDI *	**Mean diameter (nm)** †
Mean	0.072	25.09
S.D.	0.034	0.21
	TRAP-cage^{DTME}	
Mean	0.098	24.80
S.D.	0.041	0.36

* PDI = Polydispersity index; † average size based on volume distribution

Table S4. Right/low angle light scattering measurements

	TRAP cage^{DTME}		TRAP cage^{BMH}	
Sample no.*	1	2	1	2
RV (ml)	12.12	11.3	11.91	11.47
Mw (g/mol)	2 220 000	2 225 000	2 255 000	2 199 000
Frac. of sample (%)	100	100	100	100
RI peak (mV·ml)	77.53	151.7	99.08	156.8
RALS peak (mV·ml)	599.1	1218	764.4	1244
LALS peak (mV·ml)	462.1	1210	593.9	1300

***** Columns 1 and 2 represent samples from a different batch of the protein at the same concentration

Table S5. Cryo-EM data collection, refinement statistics for TRAP-cage^{BMH}

	LH Cage (EMD-11413)	RH Cage (EMD-11412)
Data collection and processing		
Magnification	75000	75000
Voltage (kV)	300	300
Total exposure (e–/Å^2)	40	40
Defocus range (μm)	-1.0 ÷ -3.0	-1.0 ÷ -3.0
Pixel size (Å)	1.065	1.065
Symmetry imposed	O	O
Initial particle images (no.)	10169	10169
Final particle images (no.)	9929	9929
Map resolution (Å)	6.8	6.9
FSC threshold	0.143	0.143

Table S6. Cryo-EM data collection, refinement statistics for TRAP-cage^{DTME}

	LH Cage (EMD-11415)	RH Cage (EMD-11414)
Data collection and processing		
Magnification	75000	75000
Voltage (kV)	300	300
Total exposure (e–/Å2)	40	40
Defocus range (μm)	-1.0 ÷ -3.0	-1.0 ÷ -3.0
Pixel size (Å)	1.065	1.065
Symmetry imposed	O	O
Initial particle images (no.)	4942	4942
Final particle images (no.)	4907	4907
Map resolution (Å)	4.7	4.9
FSC threshold	0.143	0.143

Movie S1.
High-speed atomic force microscopy (HS-AFM) movie frames, taken at 2 frames per second, 200 nm x 200 nm, 200 pixel x 200 pixel, showing the effect of 4 mM DTT addition to TRAP-cage^{DTME}. Time stamp in the upper left corner of each AFM image indicates time after DTT addition. Scale bar at t = -01:23.0 indicates 50 nm. Z color scale is set to -1 nm to 16 nm. Movie is corrected for minor lateral drift. This movie plays at 25 times the original speed.

Movie S2.
High-speed atomic force microscopy (HS-AFM) movie frames, taken at 2 frames per second, 300 nm x 300 nm, 150 pixel x 150 pixel, showing the effect of 4 mM DTT addition to TRAP-cage^{BMH}. Time stamp in the upper left corner of each AFM image indicates time after DTT addition. Scale bar at t = -00:42.0 indicates 50 nm. Z color scale is set to 0 nm to 22 nm. This movie plays at 25 times the original speed.

Movie S3.
High-speed atomic force microscopy (HS-AFM) movies frames, taken at 1 frames per second, 600 nm x 600 nm, 200 pixel x 200 pixel, showing the effect of 10 mM DTT addition to TRAP-cage^{DTME} versus control. Movie on the left is TRAP-cage^{DTME} in the absence of DTT whereas the movie on the right is taken with the addition of 10 mM DTT at t = 4s. Scale bar at t = 0s indicates 100 nm. Z color scale is set to 0 nm to 20 nm. This movie plays at 50 times the original speed. The movie on the right stops at t = 548s whereas the control movie on the left continue until t = 1012s.

REFERENCES AND NOTES

1. W. M. Aumiller, M. Uchida, T. Douglas, Protein cage assembly across multiple length scales. *Chem. Soc. Rev.* **47**, 3433–3469 (2018).

2. A. Liu, C. H. H. Traulsen, J. J. L. M. Cornelissen, Nitroarene reduction by a virus protein cage based nanoreactor. *ACS Catal.* **6**, 3084–3091 (2016).

3. P. C. Jordan, D. P. Patterson, K. N. Saboda, E. J. Edwards, H. M. Miettinen, G. Basu, M. C. Thielges, T. Douglas, Self-assembling biomolecular catalysts for hydrogen production. *Nat. Chem.* **8**, 179–185 (2016).

4. B. Maity, K. Fujita, T. Ueno, Use of the confined spaces of apo-ferritin and virus capsids as nanoreactors for catalytic reactions. *Curr. Opin. Chem. Biol.* **25**, 88–97 (2015).

5. M. Lach, M. Künzle, T. Beck, Free-standing metal oxide nanoparticle superlattices constructed with engineered protein containers show in crystallo catalytic activity. *Chem. A Eur. J.* **23**, 17482–17486 (2017).

6. S. Chakraborti, A. Korpi, M. Kumar, P. Stępień, M. A. Kostiainen, J. G. Heddle, Three-dimensional protein cage array capable of active enzyme capture and artificial chaperone activity. *Nano Lett.* **19**, 3918–3924 (2019).

7. Y. Wang, T. Douglas, Protein nanocage architectures for the delivery of therapeutic proteins. *Curr. Opin. Colloid Interface Sci.* **51**, 101395 (2021).

8. M. Vujadinovic, J. Vellinga, Progress in adenoviral capsid-display vaccines. *Biomedicine* **6**, 81 (2018).

9. S. Das, L. Zhao, S. N. Crooke, L. Tran, S. Bhattacharya, E. A. Gaucher, M. G. Finn, Stabilization of near-infrared fluorescent proteins by packaging in virus-like particles. *Biomacromolecules* **21**, 2432–2439 (2020).

10. K. Majsterkiewicz, Y. Azuma, J. G. Heddle, Connectability of protein cages. *Nanoscale Adv.* **2**, 2255–2264 (2020).

11. I. Stupka, J. G. Heddle, Artificial protein cages – inspiration, construction, and observation. *Curr. Opin. Struct. Biol.* **64**, 66–73 (2020).

12. T. G. W. Edwardson, T. Mori, D. Hilvert, Rational engineering of a designed protein cage for siRNA delivery. *J. Am. Chem. Soc.* **140**, 10439–10442 (2018).

13. J. Marcandalli, B. Fiala, S. Ols, M. Perotti, W. de van der Schueren, J. Snijder, E. Hodge, M. Benhaim, R. Ravichandran, L. Carter, W. Sheffler, L. Brunner, M. Lawrenz, P. Dubois, A. Lanzavecchia, F. Sallusto, K. K. Lee, D. Veesler, C. E. Correnti, L. J. Stewart, D. Baker, K. Loré, L. Perez, N. P. King, Induction of potent neutralizing antibody responses by a designed protein nanoparticle vaccine for respiratory syncytial virus. *Cell* **176**, 1420–1431.e17 (2019).

14. J. E. Padilla, C. Colovos, T. O. Yeates, Nanohedra: Using symmetry to design self assembling protein cages, layers, crystals, and filaments. *Proc. Natl. Acad. Sci. U.S.A.* **98**, 2217–2221 (2001).

15. Y.-T. Lai, D. Cascio, T. O. Yeates, Structure of a 16-nm cage designed by using protein oligomers. *Science* **336**, 1129–1129 (2012).

16. Y. Hsia, J. B. Bale, S. Gonen, D. Shi, W. Sheffler, K. K. Fong, U. Nattermann, C. Xu, P.-S. Huang, R. Ravichandran, S. Yi, T. N. Davis, T. Gonen, N. P. King, D. Baker, Design of a hyperstable 60-subunit protein icosahedron. *Nature* **535**, 136–139 (2016).

17. N. P. King, J. B. Bale, W. Sheffler, D. E. McNamara, S. Gonen, T. Gonen, T. O. Yeates, D. Baker, Accurate design of co-assembling multi-component protein nanomaterials. *Nature* **510**, 103–108 (2014).

18. J. B. Bale, S. Gonen, Y. Liu, W. Sheffler, D. Ellis, C. Thomas, D. Cascio, T. O. Yeates, T. Gonen, N. P. King, D. Baker, Accurate design of megadalton-scale two-component icosahedral protein complexes. *Science* **353**, 389–394 (2016).

19. D. J. E. Huard, K. M. Kane, F. A. Tezcan, Re-engineering protein interfaces yields copper-inducible ferritin cage assembly. *Nat. Chem. Biol.* **9**, 169–176 (2013).

20. A. S. Cristie-David, E. N. G. Marsh, Metal-dependent assembly of a protein nano-cage. *Protein Sci.*

28, 1620–1629 (2019).

21. E. Golub, R. H. Subramanian, J. Esselborn, R. G. Alberstein, J. B. Bailey, J. A. Chiong, X. Yan, T. Booth, T. S. Baker, F. A. Tezcan, Constructing protein polyhedra via orthogonal chemical interactions. *Nature* **578**, 172–176 (2020).

22. A. A. Antson, J. Otridge, A. M. Brzozowski, E. J. Dodson, G. G. Dodson, K. S. Wilson, T. Smith, M. Yang, T. Kurecki, P. Gollnick, The structure of trp RNA-binding attenuation protein. *Nature* **374**, 693–700 (1995).

23. M. Imamura, T. Uchihashi, T. Ando, A. Leifert, U. Simon, A. D. Malay, J. G. Heddle, Probing structural dynamics of an artificial protein cage using high-speed atomic force microscopy. *Nano Lett.* **15**, 1331–1335 (2015).

24. A. D. Malay, J. G. Heddle, S. Tomita, K. Iwasaki, N. Miyazaki, K. Sumitomo, H. Yanagi, I. Yamashita, Y. Uraoka, Gold nanoparticle-induced formation of artificial protein capsids. *Nano Lett.* **12**, 2056–2059 (2012).

25. A. D. Malay, N. Miyazaki, A. Biela, S. Chakraborti, K. Majsterkiewicz, I. Stupka, C. S. Kaplan, A. Kowalczyk, B. M. A. G. Piette, G. K. A. Hochberg, D. Wu, T. P. Wrobel, A. Fineberg, M. S. Kushwah, M. Kelemen, P. Vavpetič, P. Pelicon, P. Kukura, J. L. P. Benesch, K. Iwasaki, J. G. Heddle, An ultra-stable gold-coordinated protein cage displaying reversible assembly. *Nature* **569**, 438–442 (2019).

26. R. Zschoche, D. Hilvert, Diffusion-limited cargo loading of an engineered protein container. *J. Am. Chem. Soc.* **137**, 16121–16132 (2015).

27. Y. Azuma, M. Herger, D. Hilvert, Diversification of protein cage structure using circularly permuted subunits. *J. Am. Chem. Soc.* **140**, 558–561 (2018).

28. A. O'Neil, P. E. Prevelige, G. Basu, T. Douglas, Coconfinement of fluorescent proteins: Spatially enforced communication of GFP and mCherry encapsulated within the P22 capsid. *Biomacromolecules* **13**, 3902–3907 (2012).

29. Y. Azuma, R. Zschoche, M. Tinzl, D. Hilvert, Quantitative packaging of active enzymes into a protein cage. *Angew. Chem. Int. Ed.* **55**, 1531–1534 (2016).

30. N. H. Dashti, R. S. Abidin, F. Sainsbury, Programmable in vitro coencapsidation of guest proteins for intracellular delivery by virus-like particles. *ACS Nano* **12**, 4615–4623 (2018).

31. N. C. Shaner, M. Z. Lin, M. R. McKeown, P. A. Steinbach, K. L. Hazelwood, M. W. Davidson, R. Y. Tsien, Improving the photostability of bright monomeric orange and red fluorescent proteins. *Nat. Methods* **5**, 545–551 (2008).

32. R. Frey, S. Mantri, M. Rocca, D. Hilvert, Bottom-up construction of a primordial carboxysome mimic. *J. Am. Chem. Soc.* **138**, 10072–10075 (2016).

33. T. Ando, T. Uchihashi, T. Fukuma, High-speed atomic force microscopy for nano-visualization of dynamic biomolecular processes. *Prog. Surf. Sci.* **83**, 337–437 (2008).

34. T. Ando, T. Uchihashi, S. Scheuring, Filming biomolecular processes by high-speed atomic force microscopy. *Chem. Rev.* **114**, 3120–3188 (2014).

35. A. Miyagi, S. Scheuring, A novel phase-shift-based amplitude detector for a high-speed atomic force microscope. *Rev. Sci. Instrum.* **89**, 083704 (2018).

36. A. Miyagi, S. Scheuring, Automated force controller for amplitude modulation atomic force microscopy. *Rev. Sci. Instrum.* **87**, 053705 (2016).

37. P. Thevenaz, U. E. Ruttimann, M. Unser, A pyramid approach to subpixel registration based on intensity. *IEEE Trans. Image Process.* **7**, 27–41 (1998).

38. S. Q. Zheng, E. Palovcak, J.-P. Armache, K. A. Verba, Y. Cheng, D. A. Agard, MotionCor2: Anisotropic correction of beam-induced motion for improved cryo-electron microscopy. *Nat. Methods* **14**, 331–332 (2017).

39. A. Rohou, N. Grigorieff, CTFFIND4: Fast and accurate defocus estimation from electron micrographs. *J. Struct. Biol.* **192**, 216–221 (2015).

40. A. Punjani, J. L. Rubinstein, D. J. Fleet, M. A. Brubaker, cryoSPARC: Algorithms for rapid unsupervised cryo-EM structure determination. *Nat. Methods* **14**, 290–296 (2017).

41. H. Schägger, Tricine-SDS-PAGE. *Nat. Protoc.* **1**, 16–22 (2006).

42. C. Vallance, “Introduction to Complex Reactions” in *An Introduction to Chemical Kinetics* (IOP Publishing, 2017); http://dx.doi.org/10.1088/978-1-6817-4664-7, chap. 5.